Kinetics and spatial organization in reactive systems with nonpassively advected reactants

2007 J. Phys.: Condens. Matter 19 065132

(http://iopscience.iop.org/0953-8984/19/6/065132)

INSTITUTE OF PHYSICS PUBLISHING JOURNAL OF PHYSICS: CONDENSED MATTER

J. Phys.: Condens. Matter **19** (2007) 065132 (10pp) doi:10.1088/0953-8984/19/6/065132

Kinetics and spatial organization in reactive systems with nonpassively advected reactants

R Reigada[1], **F Sagués**[1] **and J M Sancho**[2]

[1] Departament de Química Física, Universitat de Barcelona, Avgda. Diagonal 647, Barcelona 08028, Spain
[2] Departament d'Estructura i Constituents de la Matèria, Universitat de Barcelona, Avgda. Diagonal 647, Barcelona 08028, Spain

Received 17 July 2006
Published 22 January 2007
Online at stacks.iop.org/JPhysCM/19/065132

Abstract

A reactive system under the influence of a turbulent flow leads to a diversity of kinetic regimes that result from the interplay between reaction, advection and drag forces. Inertial bias collects reactants preferentially in certain regions of the flow depending on their density, and this fact strongly determines the overall kinetic behaviour and the spatial organization of the reactive mixture. We present a Eulerian scheme for the advection terms in a kinetic mean-field model that is better suited to the study of nonpassively advected reactive systems than the original Lagrangian approach. We show two examples of these systems: first, a formal study of the typical binary diffusion-controlled reaction $A + B \rightarrow 0$, when the reactants are nonpassively advected; second, application to the study of plankton dynamics in the ocean that reproduces the well-known periodically sustained plankton blooms.

1. Introduction

Advection of particles by turbulent flows can be considered as one of the most interesting problems in fluid mechanics, and a basic issue in environmental and engineering fields. The mixing efficiency of such flows has been an object of study for years and the idea that turbulence is a good mixing mechanism is today inconsistent with experimental observations that show the existence of particle aggregation patterns even in the strongest turbulent flows. This is related to the fact that turbulent flows are clearly characterized by structure and underlying coherence [1]. This aggregation phenomenon is even more dramatic when considering nonpassively advected particles. In this case, particles do not follow the flow lines of the fluid exactly, and therefore, even under incompressible flow, an initially homogenized condition segregates and particles tend to accumulate in certain regions of the advecting field [2].

Patterning due to the motion of nonpassive particles in a turbulent fluid is crucial for the understanding of a large variety of problems like the settling of aerosol particles [3, 4], the dispersion of pollutants in the atmosphere, the distribution of planktonic organisms in the

ocean [5], etc. More specifically, when advected particles are involved in a reactive process, the induced structural organization and the reactive kinetics are strongly connected and may lead to nontrivial or complex behaviours. As a formal example, let us consider the reaction $A + B \to 0$ [6, 7]. When diffusion is not an efficient mixing mechanism (for instance in low dimensions), initial inhomogeneous fluctuations evolve, giving rise to clusters (of either A or B) that grow with time [8, 9] and, since the reaction only takes place at the cluster's boundaries, the rate law is slower than the classical one. Passive turbulent mixing procedures are known to restore for a while the classical (fast) kinetic regime [10, 11]. However, when nonpassive advection is considered, induced reactant aggregation may result in a large variety of kinetic behaviours that spans from classical kinetics to complete reaction stoppage [12].

Another example of the influence of nonpassive turbulence can be found in the study of planktonic dynamics in the ocean. All oceanic organisms experience advection by turbulence which can cause inhomogeneous spatial distributions. More specifically, phytoplankton and zooplankton have different viscous and inertial properties, so that they may accumulate in separate areas of the flow [13]. Phytoplankton–zooplankton interactions can be treated like prey–predator dynamics through an elementary excitable reactive scheme. A simple model [14] demonstrates that the interplay between differential flow effects of the planktonic species and the excitable reaction dynamics may reproduce the observed oceanic phytoplankton blooms and patchiness.

Lots of numerical and analytical approaches have been devoted to the study of the motion of particles in turbulent flow fields. In this paper, we revisit this problem using as an advection field a synthetic, two-dimensional turbulent flow with some prescribed statistical properties. In section 2.1 we present the flow and a brief introduction to the procedure through which we generate it. Although the most visual approach to studying particle advection is by means of a Lagrangian prescription, we rather prefer to use an Eulerian model for the inertial terms compatible with the continuum prescription mostly used to study reaction–diffusion problems. This approach is presented and numerically tested in section 2.2. The rest of the paper is devoted to reviewing the main results obtained by application of the Eulerian prescription to the two aforementioned problems. On the one hand, in section 3 we revisit the diffusion–reaction–advection problem for nonpassively advected reactants, and a detailed study of the kinetic regimes is presented for the $A + B \to 0$ reaction. On the other hand, the main results of our research on planktonic dynamics are presented in section 4. Finally, section 5 summarizes our findings and conclusions.

2. Numerical methods

2.1. Synthetic turbulent velocity flow

To mimic turbulent mixing conditions, we generate a statistically homogeneous, isotropic and stationary two-dimensional velocity field, $\mathbf{U}(x, y)$, as first proposed in [15]. This represents a 'synthetic' turbulent flow with some prescribed statistical properties; u_0^2 denotes its intensity, and l_0 and t_0 its length and time correlation, respectively. These kinematic characteristics are expressed in terms of the velocity correlation function, which in turn depends on the form of the energy spectrum. For the flow used in our research we have adopted Kraichnan's spectrum [16], as it describes a turbulent flow that incorporates a wide band of excited modes, but whose energy drops off sharply for large wavenumbers.

A detailed presentation of the algorithm can be found in [15]. The whole procedure is discretized ($\mathbf{U}_{i,j}$) in space using a square lattice of $N \times N$ points and unit spacing Δx, so that the linear size of the system is $L = N\Delta x$. For the sake of simplicity, and in order to avoid

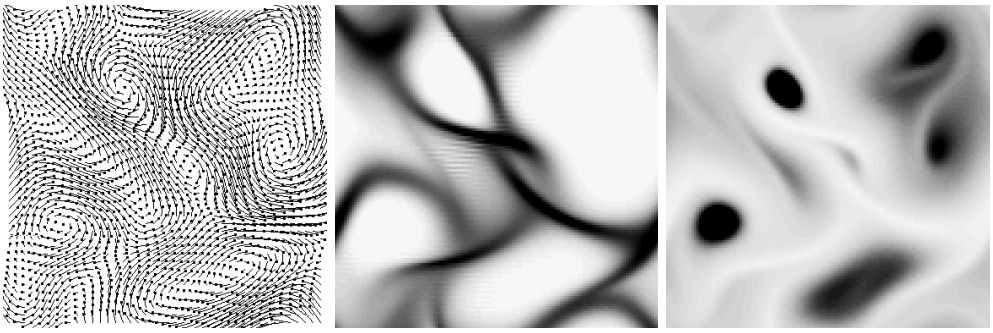

Figure 1. Left: turbulent velocity field, $\mathbf{U}_{i,j}$, with $u_0^2 = 1$ and $l_0 = 6$ used in some of the simulations in this paper. Middle and right: concentration plots at $t = 180$ for $D = 0.25$ and $A = 6$ for the velocity flow in the left panel. The middle panel corresponds to heavy particles ($\beta = 0$) and the right panel to light particles ($\beta = 2$).

the existence of a great number of temporal scales, we consider a frozen flow, so we have fixed $t_0 = \infty$ in our flow simulations. In the left panel of figure 1 we show an example of the velocity field obtained by the algorithm presented.

2.2. Eulerian scheme

Since our main interest on what follows consists of incorporating reaction effects affecting dispersed particles, we use a continuum scheme of particle concentrations instead of the more visual particle description. The inclusion of reactive terms is rather easy to implement in terms of advection–diffusion–reaction equations for particle concentrations. For a single component system,

$$\frac{\partial c(\mathbf{r},t)}{\partial t} = -\nabla \cdot \mathbf{v}(\mathbf{r},t)c(\mathbf{r},t) + D\nabla^2 c(\mathbf{r},t), \tag{1}$$

where $c(\mathbf{r},t)$ corresponds to the local concentration, D the diffusion constant, and $\mathbf{v}(\mathbf{r},t)$ the velocity of the particles at the position $\mathbf{r}$ at time t. This velocity is related to the fluid velocity field as [17]

$$\frac{\partial \mathbf{v}(\mathbf{r},t)}{\partial t} = \alpha(\mathbf{U}(\mathbf{r}) - \mathbf{v}(\mathbf{r},t)) - (\mathbf{v}(\mathbf{r},t)\cdot\nabla)\,\mathbf{v}(\mathbf{r},t) + \beta(\mathbf{U}(\mathbf{r})\cdot\nabla)\mathbf{U}(\mathbf{r}). \tag{2}$$

Here, $\alpha = Al_0/u_0$ is the dimensionless version of the inertia parameter, and $A = (12\pi a\mu)/(2m_p + m_f)$ sets the balance between viscous and inertial forces. The Bernouilli parameter $\beta = 3m_f/(2m_p + m_f)$ introduces the ratio between m_p, the particle mass, and m_f the mass of the volume of fluid displaced by the particle, μ is the dynamic viscosity associated with the surrounding fluid, and a is the radius of the particle. We have rescaled space, time and velocity by the scale factors l_0, l_0/u_0 and u_0. We have to be aware of the limitations of equation (2), since it implicitly assumes the existence of a particle velocity field; namely, that the velocity of a particle is determined only by its position. This is guaranteed by assuming that the viscous term dominates the inertial forces ($\alpha \gg 1$) in such a way that the history (trajectory) of the particle is not necessary to know its actual velocity. This is only valid under the conditions used in the asymptotical approach developed in [17] and references therein.

To check numerically the validity of this field prescription, we discretize and solve equations (1) and (2). Discretization of an advection term is technically rather complicated, especially in systems leading to aggregation, since high concentration gradients appear.

After comparing different explicit methods, we finally choose the two-step Lax–Wendroff scheme [18], with a time step $\Delta t = 0.0002$ which gives us good numerical accuracy. We start from a random initial distribution of local concentrations, and periodic boundary conditions apply. The middle and right panels of figure 1 show the concentration distributions for heavy particles (middle) and light particles (right) for a given diffusion constant $D = 0.25$. Grey scales have been used here: black for the higher concentrations and white for the smaller. The results obtained from this scheme show the same aggregation behaviour as from Lagrangian simulations [17]; namely, heavy particles ($\beta < 1$) accumulate in regions with low vorticity and high strain rate, whereas light particles ($\beta > 1$) collect in zones with high vorticity and low strain rate.

3. $A + B \to 0$ reactive system

We now address one of the two examples of interest in this paper: the diffusion–advection problem of two species reacting according to $A + B \to 0$. Our starting points are mean-field reaction–diffusion–advection equations:

$$\begin{aligned} \frac{\partial c_A(\mathbf{r},t)}{\partial t} &= -\nabla\cdot\mathbf{v}_A(\mathbf{r},t)c_A(\mathbf{r},t) + D\nabla^2 c_A(\mathbf{r},t) - kc_A(\mathbf{r},t)c_B(\mathbf{r},t) \\ \frac{\partial c_B(\mathbf{r},t)}{\partial t} &= -\nabla\cdot\mathbf{v}_B(\mathbf{r},t)c_B(\mathbf{r},t) + D\nabla^2 c_B(\mathbf{r},t) - kc_A(\mathbf{r},t)c_B(\mathbf{r},t). \end{aligned} \tag{3}$$

The numerical discretization of equations (3) and (2) follows the same prescription as in section 2.2. A random and stoichiometric distribution for the initial local concentrations is chosen ($\langle c_A\rangle = \langle c_B\rangle = \langle c\rangle = 1$). Since we want to keep ourselves to a diffusion-controlled situation, we usually take small values for the diffusion coefficient ($D = 0.1$) and a much larger value for the reaction constant ($k = 2$).

The case without advection shows the typical asymptotic diffusion-limited kinetics, $c \sim t^{-1/2}$ (for two-dimensional systems). When including passive advection ($\mathbf{v}_A(\mathbf{r},t) = \mathbf{v}_B(\mathbf{r},t) = \mathbf{U}(\mathbf{r})$) the system first enters a mixing-aided regime where the classical kinetics $c \sim t^{-1}$ is transiently restored. The length scale of this regime is dictated by the correlation length of the flow. When the diffusion length becomes larger, the system crosses over to a diffusion-controlled regime $t^{-1/2}$, where the anomalous kinetics shows up again [10, 11]. In figure 2 these two behaviours are readily recognized as reference cases to be used later on.

The effect of nonpassive advection on the reaction kinetics, assuming large and equal values of α, depends on the densities of the reactant species (β_i). Here, two extreme scenarios are presented, depending on whether both species have the same density or strongly different densities. Intermediate cases are believed to not show any different qualitative behaviour.

When both species have the same density we generally observe an enlargement of the classical $c \sim t^{-1}$ law in relation to the passively advected cases. This effect is already shown for very light particles ($\beta_A = \beta_B = 2$) but it is far more evident for very heavy particles ($\beta_A = \beta_B = 0$). Obviously, this effect is reduced when the densities of the two species approach that of the fluid ($\beta_i \to 1$). We define an effective reaction rate k_{eff} during the inertia-induced classical stage of the reaction from a fit to $c^{-1} = a_0 + k_{\text{eff}}t$. Generally, the values of k_{eff} are closer to k when the reactants are nonpassively advected, especially if both species are lighter than the fluid. For instance, for the cases plotted in figure 2 where $k = 2$, $k_{\text{eff}} = 0.737$ for the passively advected case, $k_{\text{eff}} = 1.356$ for the case of heavy particles and $k_{\text{eff}} = 1.421$ for the case of light particles.

In spite of the fact that nonpassive advection effects first enhance the reactive process, at longer times the system becomes strongly segregated (see figure 3) and a very slow decay is found (actually the reaction is almost halted). This effect is more dramatic and shows up earlier

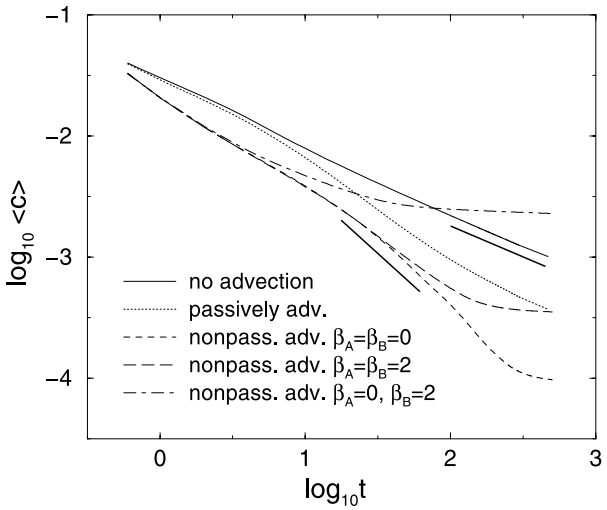

Figure 2. Log–log plot for the temporal evolution of $\langle c \rangle$ for different binary reacting systems analysed in this paper. $k = 2$ and $D = 0.1$ in all cases. For the systems with advection, we have $u_0^2 = 1$ and $l_0 = 6$. For the cases with inertia, $\alpha = 6$. Slopes -1 and $-1/2$ are plotted to help to identify the different kinetic regimes.

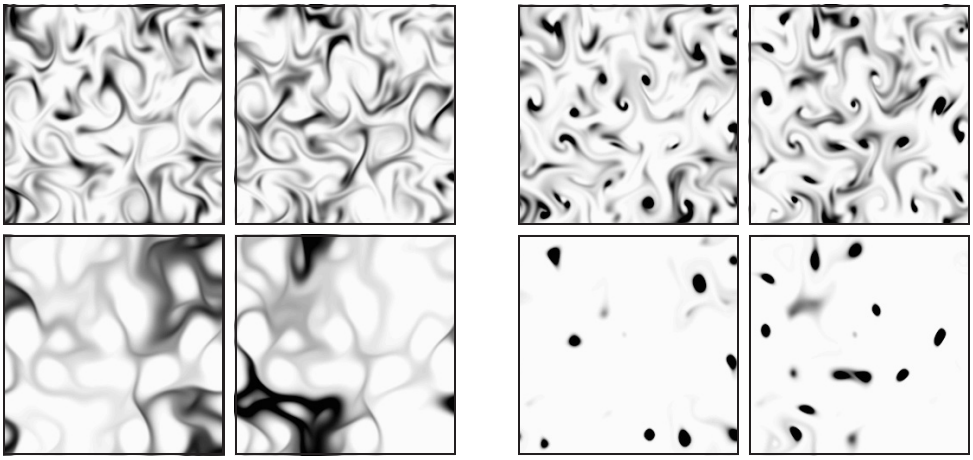

Figure 3. Concentration plots for the species A (left) and B (right) at $t = 25$ (top) and 500 (bottom) in a nonpassively advected system. The bottom plots are chosen to correspond to times when the reaction has already been halted due to the segregation of reactants. The first panel corresponds to the case where both species are heavier than the fluid ($\beta_A = \beta_B = 0$). The second panel stands for the case where both species are lighter than the fluid ($\beta_A = \beta_B = 2$). We use the same flow as in figure 4.

for light particles than for heavy ones. In any case, no purely diffusion-controlled regime is found whatsoever, since the diffusive (mixing) process is counterbalanced by the inertial drift that keeps the reactants segregated once the system enters such a slow regime. This is the first important conclusion to emphasize: stated in short and differently to the passively advected case, the transient regime of classical kinetics leads directly to a no-reaction stage, whereas the standard $t^{-1/2}$ behaviour is never observed.

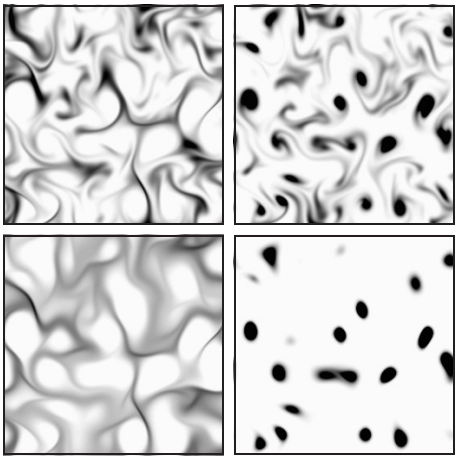

Figure 4. Concentration plots for the species A (left) and B (right) at $t = 25$ (top) and 500 (bottom) in a nonpassively advected system. One species is heavier than the fluid ($\beta_A = 0$) and the other one is lighter ($\beta_B = 2$). We use the same flow realization as in figure 3.

Before going ahead, it is worth presenting here some quantitative details of the spatial mass distribution following the reaction–diffusion–advection effects described previously. Although for the heavy reactants case the full system average concentration is quite small at $t = 500$ (the maximum time shown for our simulations), $\langle c \rangle = 10^{-4}$, half of the remaining mass is accumulated only in 10% of the system. Moreover, in some aggregation regions, the mean local concentration can be ten times larger than the whole concentration average. This effect is even more pronounced for light reactants: for a similar tiny average concentration, half of the remaining mass at $t = 500$ is concentrated in 2.5% of the system, and one can find regions inside the eddies where the local concentration exceeds one hundred times the whole concentration average.

Finally, for reactants with differential densities the accumulation in different regions due to an inertial drift in opposite directions effectively separates both reactants from the very beginning. Consequently, the kinetic decay is strongly slowed down already at very early times. The decay curve for this case is also plotted in figure 2, and the corresponding concentration evolution is shown in figure 4 for the same realization of the flow as in figure 3. The decay law in this case follows the classical t^{-1} behaviour but very prematurely; even well before consuming most of the reactants, it is completely stopped.

4. Plankton dynamics

Plankton patchiness has been observed on a wide range of spatial and temporal scales [13, 19, 20] and has been attributed to a range of physical and biological mechanisms. It is important to understand both the mechanisms that result in patchiness and the effect of patchiness on food–web interactions, which can have a major impact on fisheries policy [21]. Moreover, at moderate spatial scales, phytoplankton 'blooms' can occur, whereby the population of phytoplankton rapidly increases in number and remains at this level for some period of time before returning to normal. This is the hallmark of an excitable system. Truscott and Brindley investigated a two-component phytoplankton–zooplankton (PZ) model which has the characteristics of an excitable system whose excitability is robust over a realistic parameter range [22].

In our study of planktonic dynamics we have conjectured that the differential flow of phytoplankton and zooplankton is sufficient to seed a bloom [14]. This scenario requires no extraneous perturbation to drive the excitation. In other words, after sufficient inertial separation a large population of phytoplankton might be allowed to grow in certain localized regions with minimal predation and this, coupled with dispersive effects, may constitute the supra-threshold perturbation necessary for an excitable system.

To model plankton dynamics we use a Holling type III grazing by zooplankton and a linear higher-predatory response with regard to the zooplankton mortality [22]:

$$\begin{aligned} \mathcal{I}_P(P, Z) &= rP\left(1 - \frac{P}{K}\right) - \frac{\gamma Z P^2}{P^2 + \kappa^2}, \\ \mathcal{I}_Z(P, Z) &= \frac{e\gamma Z P^2}{P^2 + \kappa^2} - \delta Z, \end{aligned} \tag{4}$$

where P and Z are the phytoplankton and zooplankton concentrations, respectively.

We further couple the above rate laws to an advection–diffusion scheme. We nondimensionalize the resulting equations such that $P = Kp$, $Z = Kz$, $x = l_0\tilde{x}$, $y = l_0\tilde{y}$, $t = \tau l_0/u_0$, $\mathbf{V}^i = u_0\mathbf{v}^i$, and $d_i = D_i/(u_0 l_0)$, with $\mathbf{V}^i$ obtained from equation (2) with appropriate choices of $\beta = \beta_p$ and β_z, and D_i representing turbulent diffusivities (assumed to be equal; see below). After dropping the tildes, this gives us the following nondimensional scheme:

$$\begin{aligned} \frac{\partial p}{\partial \tau} &= -\nabla \cdot (\mathbf{v}^p p - d_p \nabla p) + \omega p(1 - p) - \frac{\bar{\gamma} z p^2}{p^2 + \chi^2}, \\ \frac{\partial z}{\partial \tau} &= -\nabla \cdot (\mathbf{v}^z z - d_z \nabla z) + \epsilon\left(\frac{\bar{\gamma} z p^2}{p^2 + \chi^2} - \sigma z\right), \end{aligned} \tag{5}$$

where the dimensionless parameters of the excitable model are defined to be $\omega = rl_0/u_0$, $\epsilon = e$, $\chi = \kappa/K$, $\sigma = \delta l_0/(\epsilon u_0)$ and $\bar{\gamma} = \gamma l_0/u_0$.

In order to obtain results on the correct length and time scales, we select our model parameters to be as realistic as possible. We choose L, the simulation box size, to be 50 km (where l_0 is related to L in the sense that l_0 determines the scale of the eddies, and in this case we choose $L \approx 10\, l_0$; see figure 1) and the characteristic velocity to be $u_0 = 0.1$ m s^{-1}, similar to that used in [13, 23]. From [22], we take $\omega = 0.162$, $\chi = 0.053$, $\sigma = 0.130$ and $\epsilon = 0.05$ (hence, the zooplankton population is the slow/recovery variable). Our choices of l_0 and u_0 are such that we can realistically fix $\bar{\gamma} = 1$ and, hence, the reaction effects are comparable to advective effects. In line with a realistic range of values for the inertial parameters [5] we assume, henceforth, that $A = 0.0257$ s^{-1}, which means that the zooplankton radius is approximately 1 cm and implies that $\alpha \gg 1$, justifying the preceding asymptotic analysis.

Kraichnan's spectrum used in our synthetic turbulent flow has a maximum occurring at $k = 0.75$ and drops to a very small value at $k = 2$. Hence, the length scale associated with the highest energy is equal to $2\pi/0.75 = 8.4$, or about a tenth of the length of the simulation region. The length scale associated with a wavenumber of 2 (residual energy) is given by π, or about one 20th of the simulation region. If the simulation region is 50 km, then the dimensional length scale associated with low spectral energy is $L/20 = 2.5 \times 10^5$ cm. This is the length scale for which we wish to implement a turbulent diffusivity in the reaction–advection–diffusion system. Hence, the diffusivity $D = 0.01 * l^{1.15} = 1.6 \times 10^4$ cm^2 s^{-1} $= 1.6$ m^2 s^{-1} (according to the empirical relationship extracted by Okubo from experimental data [24]). For the numerical resolution of equations (2) and (5) we follow the same discretization procedure and numerical scheme presented in the previous sections. We begin from a homogeneous initial distribution of both species in their unexcited, equilibrium concentration values $p^* = 0.038\,27$ and $z^* = 0.046\,03$.

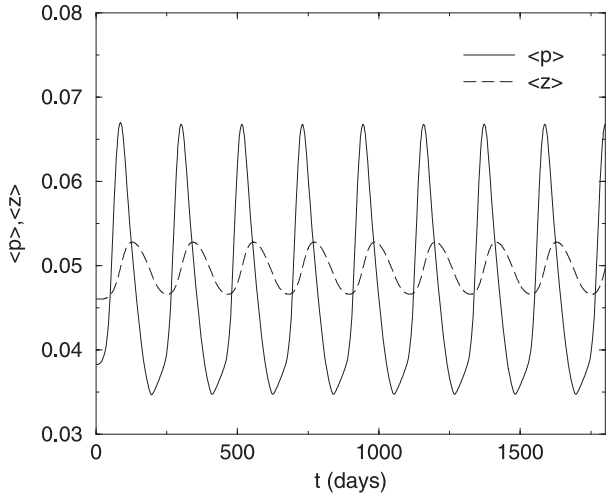

Figure 5. Oscillatory bloom in the mean concentrations of phytoplankton and zooplankton.

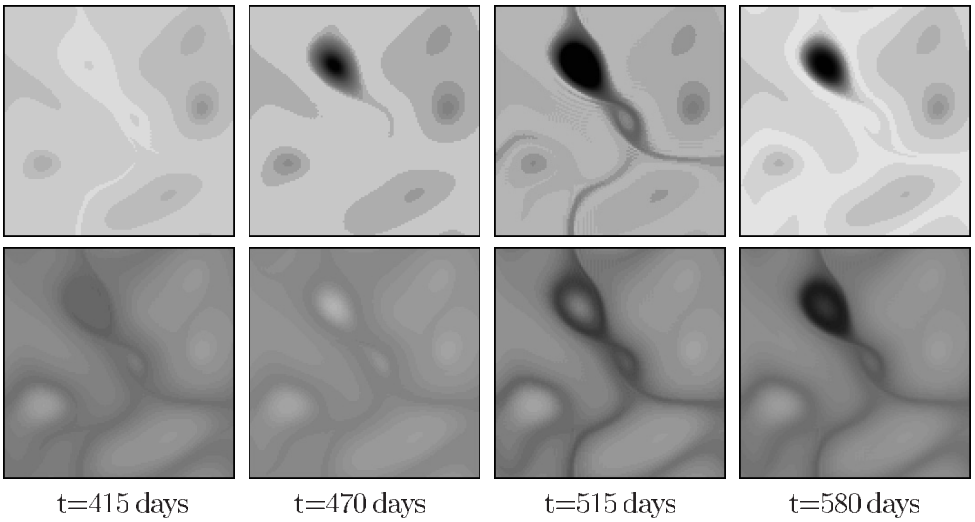

Figure 6. Snapshots of the phytoplankton (top) and zooplankton (bottom) distribution during the oscillatory bloom. For snapshots of phytoplankton, white refers to $p = 0$, and for p greater than or equal to 0.6 black is used. For zooplankton, white refers to $z = 0$ and black implies that z is greater than or equal to 0.1.

The most interesting cases occurs for the regime where we have neutrally buoyant phytoplankton ($\beta_p = 1$) and slightly heavy zooplankton ($\beta_z = 0.9$). Here, we indeed see the emergence of an oscillatory bloom in the average phytoplankton population with a period of around 210 days. Figure 5 presents the nature of the oscillatory bloom in the mean population values of phytoplankton and zooplankton, whereas in figure 6 one may observe the spatial evolution of the distribution of the phytoplankton population during one bloom cycle. What is fascinating is that this regime is the most physically realistic scenario, as phytoplankton are usually close to neutrally buoyant and zooplankton are slightly more dense than the surrounding ocean [5, 20].

A detailed observation of the planktonic dynamics reveals the inertial-induced mechanism leading to an oscillatory behaviour [14]. The initial excitation is due to the inertial drift of zooplankton that move out from the eddies, initiating a phytoplankton bloom inside the vortices. At this initial stage, the phytoplankton population increases and spreads (diffuses) inside the vortices unoccupied by zooplankton, which in turn decreases in the whole system due to the lack of prey. Later on, the zooplankton starts to grow due to the presence of large quantities of phytoplankton, especially in the straining regions of the flow around the eddies where the phytoplankton had accumulated previously. At this stage, the zooplankton population penetrates (via growth and diffusion) into the eddies due to the large localized concentration of phytoplankton, counteracting the effects of inertial drift. After some time, phytoplankton is reduced to small concentrations in the centre of the vortical structures, so the zooplankton population begins to decay due to the lack of prey and move out from the eddies, reaching the initial state and completing the oscillation.

5. Conclusions

In this paper the problem of inertial reactants advected by turbulence has been studied. We apply the Eulerian prescription to our model to characterize the presence of an aggregation behaviour for heavy and light particles. Heavy particles escape from the flow eddies and circulate following thin paths between them. In contrast, light particles are attracted by the regions of turbulence with high vorticity and remain accumulated inside the vortical structures of the flow.

We consider two reactive scenarios where the inertial effects of the advected reactants strongly determine the kinetic response. First, the diffusion-controlled $A + B \rightarrow 0$ reaction, where we have distinguished two different situations. When the two reactants have the same density (either larger or smaller than the density of the fluid) the aggregation zones are common to both species, and thus the mixing efficiency of the flow is temporary increased. After some time, segregation also takes place inside the common aggregation regions, and the kinetic decay slows down dramatically. In contrast, when the two reactants have different densities (one above and the other below the fluid density), the accumulation areas for one and the other species are different as well, so the reaction is almost halted from an early time. The connection between the fast and slow kinetic regimes and the spatial patterning of the system has been also presented.

Finally, we have demonstrated how differential flow effects of planktonic species (phytoplankton and zooplankton), coupled with excitable reaction dynamics, may contribute towards oceanic phytoplankton blooms and patchiness. Of particular interest is the oscillatory excitation, which occurs in the most realistic inertial regime (neutrally buoyant phytoplankton and slightly heavy zooplankton). The important message in this work is that, with a minimal model and using experimentally determined values for the parameters, we obtain a natural period just less than one year, which may be further synchronized by external forcing (variations of temperature, light, nutrients, etc). This self-initiating, periodic patch forming mechanism differs from other related work on advection enhanced blooms [23] as it requires no initial perturbation and is self-sustaining.

Acknowledgments

We acknowledge support from the Dirección General de Investigación Científica y Técnica (Spain) under project nos BQU2003-05042-C02-01 and BF2003-07850, and from the Direcció

General de Recerca de la Generalitat de Catalunya under project no 2001SGR00045. We also thank M A Bees and R M Hillary for their contribution to the research on planktonic dynamics.

References

[1] Ottino J M 1989 *The Kinematic of Mixing: Stretching, Chaos and Transport* (Cambridge: Cambridge University Press)
[2] Squires K D and Eaton J K 1991 *Phys. Fluids* A **3** 1169
[3] Maxey M R 1987 *J. Fluid Mech.* **174** 441
[4] Wang L P and Maxey M R 1993 *J. Fluid Mech.* **256** 27
[5] Squires K D and Yamazaki H 1995 *Deep-Sea Res.* **42** 1989
[6] Ovchinnikov A A and Zeldovich Ya B 1978 *Chem. Phys.* **28** 215
[7] Kotomin E and Kuzovkov V 1996 Moderns aspects of diffusion-controlled reactions *Cooperative Phenomena in Bimolecular Processes* (Amsterdam: Elsevier)
[8] Reigada R, Sagués F, Sokolov I M, Sancho J M and Blumen A 1996 *Phys. Rev.* E **53** 3167
[9] Sancho J M, Romero A H, Lindenberg K, Sagués F, Reigada R and Lacasta A 1996 *J. Phys. Chem.* **100** 19066
[10] Reigada R, Sagués F, Sokolov I M, Sancho J M and Blumen A 1997 *Phys. Rev. Lett.* **78** 741
[11] Reigada R, Sagués F, Sokolov I M, Sancho J M and Blumen A 1997 *J. Chem. Phys.* **107** 843
[12] Reigada R, Sagués F and Sancho J M 2002 *J. Chem. Phys.* **117** 258
[13] Abraham E R 1998 *Nature* **39** 577
[14] Reigada R, Hillary R M, Bees M A, Sancho J M and Sagués F 2003 *Proc. R. Soc.* B **270** 875
[15] Martí A C, Sancho J M, Sagués F and Careta A 1997 *Phys. Fluids* **9** 1078
[16] Kraichnan R H 1970 *Phys. Fluids* **13** 22
[17] Reigada R, Sagués F and Sancho J M 2001 *Phys. Rev.* E **64** 026307
[18] *Numerical Recipes in C* 1992 2nd edn (Cambridge: Cambridge University Press)
[19] Franks P J S 1997 *Limnol. Oceanogr.* **42** 1297
[20] Folt C L and Burns C W 1999 *Trends Ecol. Evol.* **14** 300
[21] Legendre L 1990 *J. Plankton Res.* **12** 681
[22] Truscott J E and Brindley J 1990 *J. Bull. Math. Biol.* **56** 981
[23] Neufeld Z, Haynes P H, Garçon V C and Sudre J 2002 *Geophys. Res. Lett.* **29** 1029
[24] Okubo A 1971 *Deep-Sea Res.* **18** 789